

# Ultrarapid Desalting of Protein Solutions for Electrospray Mass Spectrometry in a Microchannel Laminar Flow Device

Derek J. Wilson and Lars Konermann\*

Department of Chemistry, The University of Western Ontario, London, ON, N6A 5B7, Canada

The adverse effects of nonvolatile salts on the electrospray (ESI) mass spectra of proteins and other biological analytes are a major obstacle for a wide range of applications. Numerous sample cleanup approaches have been devised to facilitate ESI-MS analyses. Recently developed microdialysis techniques can shorten desalting times down to several minutes, the bottleneck being diffusion of the contaminant through a semipermeable membrane. This work introduces an approach that allows the on-line desalting of macromolecule solutions within tens of milliseconds. The device does not employ a membrane; instead, it uses a two-layered laminar flow geometry that exploits the differential diffusion of macromolecular analytes and low molecular weight contaminants. To maximize desalting efficiency, diffusive exchange between the flow layers is permitted only for such a time as to allow full exchange of salt, while incurring minimal macromolecule exchange. Computer simulations and optical studies show that the device can reduce the salt concentration by roughly 1 order of magnitude, while retaining ~70% of the original protein concentration. Application of this approach to the on-line purification of salt-contaminated protein solutions in ESI-MS results in dramatic improvements of both the signal-to-noise ratio and the absolute signal intensity. However, efficient desalting requires the diffusion coefficients of salt and analyte to differ by roughly 1 order of magnitude or more. This technique has potential to facilitate high-throughput analyses of biological macromolecules directly from complex matrixes. In addition, it may become a valuable tool for process monitoring and for on-line kinetic studies on biological systems.

Since its inception in the late 1980s, electrospray ionization mass spectrometry (ESI-MS) has become one of the most powerful and widely used bioanalytical techniques.<sup>1–3</sup> The numerous advantages of ESI-MS include high sensitivity and selectivity, ease of use, and low sample consumption. Virtually any analyte

can be monitored, including proteins, nucleic acids, and even intact noncovalent complexes.<sup>4,5</sup>

Perhaps the greatest drawback of ESI-MS is its incompatibility with nonvolatile pH buffers and salts. Solvent additives of this kind are commonly used during the isolation of biological analytes, and they are frequently employed to stabilize the native structure of biopolymers.<sup>6</sup> Although the operation of an ESI source requires the presence of trace amounts of electrolyte,<sup>7</sup> an excess amount of low molecular weight ions in the analyte solution leads to signal suppression, extensive peak tailing, and poor signal-to-noise ratio.<sup>8,9</sup> The deteriorating effects of these additives are due to a combination of factors. The production of charged salt clusters during ESI adds to the overall chemical noise in the spectrum.<sup>8–10</sup> Another problem is the occurrence of heterogeneous analyte charging and adduct formation. Both of these factors divide the overall ion abundance for a given analyte charge state among numerous peaks. For example, instead of exclusively forming  $[M + nH]^{n+}$  ions, an analyte might appear in various charged forms such as  $[M + iH + jNa + kK]^{(i+j+k)+}$ . The alkaline metal cations chiefly responsible for this effect are ubiquitous solution contaminants, which often persist even after extensive sample cleanup. The formation of charge neutral adducts, e.g., by attachment of multiple NaCl moieties to an analyte ion, can further aggravate the extent of peak splitting.<sup>11</sup> Nonvolatile salts also interfere with the ESI process directly, resulting in less effective ion desolvation and transmission.<sup>12</sup>

Numerous approaches have been proposed to overcome the salt tolerance problem in ESI-MS. Reducing the analyte solution flow rate to nanoelectrospray conditions decreases the initial size of the droplets leaving the ESI emitter, thus reducing the salt concentration process that accompanies droplet shrinkage during

\* To whom correspondence should be addressed. E-mail: konerman@uwo.ca; <http://publish.uwo.ca/~konerman/>.

- (1) Bruins, A. P.; Covey, T. R.; Henion, J. D. *Anal. Chem.* **1987**, *59*, 2642–2646.
- (2) Fenn, J. B.; Mann, M.; Meng, C. K.; Wong, S. F.; Whitehouse, C. M. *Science* **1989**, *246*, 64–71.
- (3) Fenn, J. B. *Angew. Chem., Int. Ed.* **2003**, *42*, 3871–3894.

- (4) Loo, J. A. *Int. J. Mass Spectrom.* **2000**, *200*, 175–186.
- (5) Heck, A. J. R.; Van den Heuvel, R. H. H. *Mass Spectrom. Rev.* **2004**, *23*, 368–389.
- (6) Tolic, P. L.; Bruce, J. E.; Lei, Q. P.; Anderson, G. A.; Smith, R. D. *Anal. Chem.* **1998**, *70*, 405–408.
- (7) Kebarle, P.; Tang, L. *Anal. Chem.* **1993**, *65*, 972–986.
- (8) Hao, C.; March, R. E.; Croley, T. R.; Smith, J. C.; Rafferty, S. P. *J. Mass Spectrom.* **2001**, *36*, 79–96.
- (9) Zhou, S.; Hamburger, M. *Rapid Commun. Mass Spectrom.* **1996**, *10*, 797–800.
- (10) Juraschek, R.; Dulcks, T.; Karas, M. *J. Am. Soc. Mass Spectrom.* **1999**, *10*, 300–308.
- (11) Verkerk, U. H.; Kebarle, P. *J. Am. Soc. Mass Spectrom.* **2005**, *16*, 1325–1341.
- (12) Constantopoulos, T. L.; Jackson, G. S.; Enke, C. G. *J. Am. Soc. Mass Spectrom.* **1999**, *10*, 625–634.

ESI.<sup>10</sup> Alternatively, using an emitter that is surrounded by a collateral supersonic jet of nebulizing gas provides an increased salt tolerance.<sup>13</sup> In fused-droplet ESI, the ion source region is filled with a nebulized methanol/acetic acid mixture. Droplets generated by the ESI emitter fuse with the nebulized droplets, thereby increasing desolvation efficiency and reducing the effective salt concentration.<sup>14</sup> In many cases, the appearance of ESI mass spectra from salt-contaminated solutions can be improved through the addition of an “electrospray-friendly” organic or acidic makeup solvent.<sup>15</sup> Another approach is the partial reversal of metal salt-induced signal suppression effects by addition of volatile salts such as ammonium acetate at high (several molar) concentrations.<sup>16</sup> However, as in the case of makeup solvents and fused droplet ESI, it is not clear how far the structural integrity of biological analytes can be preserved under these conditions. Consequently, these methods may not be applicable for studies in which natively like conditions must be maintained, such as in the investigation of noncovalent complexes.

The most common strategy to cope with contaminants in ESI-MS remains the incorporation of analyte-desalting steps into the ESI-MS protocol. Various methods and devices are currently being employed, including dialysis, C<sub>18</sub>-loaded pipet tips or nanospray capillaries,<sup>17</sup> reversed-phase HPLC,<sup>18,19</sup> and size exclusion chromatography.<sup>20</sup> All of these methods can be implemented off-line or on-line, though on-line coupling is generally preferred for increased speed and reproducibility. Many of these desalting procedures are time-consuming, typically requiring tens of minutes for chromatographic desalting and hours to days for conventional dialysis.

All dialysis-based methods ultimately rely on the diffusion of low molecular weight compounds from the analyte solution into a dialysis buffer. The equilibration time  $t$  required for particles undergoing free diffusion scales quadratically with the distance  $w$  that has to be traversed for equilibration to occur, and it is inversely proportional to the diffusion coefficient  $D$  ( $t \sim w^2/D$ ).<sup>21–23</sup> Consequently, the miniaturization of dialysis devices can lead to a drastic reduction in desalting times. Microdialysis systems are becoming increasingly popular for ESI-MS sample preparation.<sup>24–27</sup> These devices typically employ a flow of analyte solution that is

separated from a counterflow of dialysis buffer by a semipermeable membrane having a suitable molecular weight cutoff. Microdialysis devices are capable of performing on-line desalting within a few minutes, which represents a drastic improvement compared to many conventional desalting methods. Further reduction of the equilibration time is limited by the presence of the dialysis membrane, which prevents the free diffusion of the contaminant species.<sup>28,29</sup> While equilibration times on the order of minutes may be sufficient for many purposes, there is a range of applications that would greatly benefit from the availability of devices capable of performing desalting on a more rapid time scale. These applications include high-throughput assays, process monitoring, and ESI-MS-based kinetic studies on protein folding, enzyme catalysis, and other biochemical reactions.<sup>15,30–32</sup>

In this work, we present an approach for the ultrarapid desalting of solutions containing proteins or other biological macromolecules. The method is based on diffusive exchange between two liquid layers in a narrow laminar flow channel. Its principle of operation is similar to previously designed diffusion-based fractionation devices and filters,<sup>33–36</sup> and it is conceptually related to a recently developed microscale molecular mass sensor.<sup>37,38</sup> The device consists of a rectangular conduit with four access holes (Figure 1). A two-layered pressure-driven laminar flow is induced by injecting salt-contaminated protein solution (pink) and desalting buffer (blue) into the channel. The desalting process is based on the different diffusion coefficients of salt and protein. The salt diffuses into the buffer layer very rapidly (red arrows), whereas diffusion of the protein is much slower (green arrows). Upon choosing a suitable residence time for the solutions inside the conduit, salt-depleted protein solution can be collected through the analyte outlet, whereas most of the salt is transferred to waste. Since the flow layers are in direct contact with each other, rather than being separated by a dialysis membrane, full advantage is taken of rapid diffusion on the microscale. As a result, substantial desalting can be achieved within tens of milliseconds. Following a theoretical characterization, the current study demonstrates that coupling this device to an ESI mass spectrometer leads to dramatic improvements of protein spectra obtained from salt-contaminated solutions.

- (13) Takats, Z.; Wiseman, J. M.; Gologan, B.; Cooks, R. G. *Anal. Chem.* **2004**, *76*, 4050–4058.
- (14) Chang, D.-Y.; Lee, C.-C.; Shiea, J. *Anal. Chem.* **2002**, *74*, 2465–2469.
- (15) Wilson, D. J.; Konermann, L. *Anal. Chem.* **2004**, *76*, 2537–2543.
- (16) Iavarone, A. T.; Udekwu, O. A.; Williams, E. R. *Anal. Chem.* **2004**, *76*, 3944–3950.
- (17) Lion, N.; Gellon, J.; Jensen, H.; Girault, H. H. *J. Chromatogr., A* **2003**, *1003*, 11–19.
- (18) Niessen, W. M. *J. Chromatogr., A* **1999**, *856*, 179–197.
- (19) Abian, J.; Oosterkamp, A. J.; Gelpi, E. *J. Mass Spectrom.* **1999**, *34*, 244–254.
- (20) Cavanagh, J.; Benson, L. M.; Thompson, R.; Naylor, S. *Anal. Chem.* **2003**, *75*, 3281–3286.
- (21) Johnson, T. J.; Ross, D.; Locascio, L. E. *Anal. Chem.* **2002**, *74*, 45–51.
- (22) Knight, J. B.; Vishwanath, A.; Brody, J. P.; Austin, R. H. *Phys. Rev. Lett.* **1998**, *80*, 3863–3866.
- (23) Hertzog, D. E.; Michalet, X.; Jager, M.; Kong, X.; Santiago, J. G.; Weiss, S.; Bakajin, O. *Anal. Chem.* **2004**, *76*, 7169–7178.
- (24) Liu, C.; Wu, Q.; Harms, A. C.; Smith, R. D. *Anal. Chem.* **1996**, *68*, 3295–3299.
- (25) Benkestock, K.; Edlund, P.-O.; Roeraade, J. *Rapid Commun. Mass Spectrom.* **2002**, *16*, 2054–2059.
- (26) Canarelli, S.; Fisch, R.; Freitag, R. *J. Chromatogr., A* **2002**, *948*, 139–149.
- (27) Xu, N.; Lin, Y.; Hofstadler, S. A.; Matson, D.; Call, C. J.; Smith, R. D. *Anal. Chem.* **1998**, *70*, 3553–3556.

## EXPERIMENTAL SECTION

**Chemicals.** Horse heart cytochrome *c* (cyt *c*) and KMnO<sub>4</sub> were purchased from Sigma (St. Louis, MO). Sodium chloride

- (28) Shimizu, M.; Kanamori, T.; Sakai, K.; Igoshi, T.; Yoshida, M. *ASAIO J.* **1992**, *38*, 748–787.
- (29) Hosoya, O.; Chono, S.; Saso, Y.; Juni, K.; Morimoto, K.; Seki, T. *J. Pharm. Pharmacol.* **2004**, *56*, 1501–1507.
- (30) Wilson, D. J.; Rafferty, S. P.; Konermann, L. *Biochemistry* **2005**, *44*, (in press).
- (31) Fabris, D. *Mass Spectrom. Rev.* **2005**, *24*, 30–54.
- (32) Li, Z.; Sau, A. K.; Shen, S.; Whitehouse, C.; Baasov, T.; Anderson, K. S. *J. Am. Chem. Soc.* **2003**, *125*, 9938–9939.
- (33) Williams, S. P.; Shulamit, L.; Lenczycki, T.; Gidding, J. C. *Ind. Eng. Chem. Res.* **1992**, *31*, 2172–2181.
- (34) Yue, V.; Kowal, R.; Neargarder, L.; Bond, L.; Muettterties, A.; Parsons, R. *Clin. Chem.* **1994**, *40*, 1810–1814.
- (35) Holl, M. R.; Galambos, P.; Forster, F. K.; Brody, J. P.; Yager, P. *Proc. Am. Soc. Mech. Eng.* **1996**, *DSC 59*, 189–195.
- (36) Brody, J. P.; Yager, P. *Solid State Actuator Workshop* **1996**, 105–108.
- (37) Costin, C. D.; Olund, R. K.; Staggemeier, B. A.; Torgerson, A. K.; Synovec, R. E. *J. Chromatogr., A* **2003**, *1013*, 77–91.
- (38) Costin, C. D.; McBrady, A. D.; McDonnell, M. E.; Synovec, R. E. *Anal. Chem.* **2004**, *76*, 2725–2733.

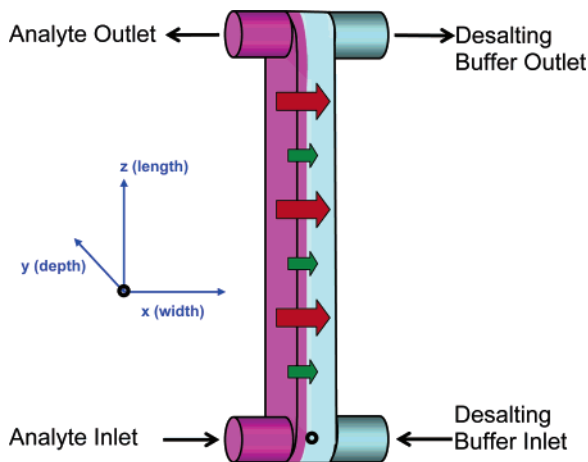


**Figure 1.** Schematic depiction of the microfluidic desalting apparatus used in this study. Pink represents the analyte stream; blue represents the desalting buffer stream. Thin arrows indicate direction of flow. Block arrows denote the rapid diffusion of salt (red) and the slow diffusion of protein (green) from the analyte solution into the desalting buffer. Also shown is the designation of  $x$ -,  $y$ -, and  $z$ -axes. The black ring denotes the origin of the Cartesian coordinate system used throughout this work.

and ammonium acetate and were obtained from Fluka (Buchs, Switzerland). Glacial acetic acid was supplied by BDH (Toronto, ON, Canada), and bradykinin was obtained from Bachem (Torrance, CA).

**Ultrarapid Desalting.** This was carried out on poly(methyl methacrylate) microchannel chips custom manufactured by Epigem (Redcar, U.K.). Each chip has a rectangular channel (length 5 in., width  $30\ \mu\text{m}$ , depth  $100\ \mu\text{m}$ ), as depicted in Figure 1. The channel ends accommodate circular access holes which, through a PEEK block adapter, can be connected to standard  $1/16$ -cm.-o.d. fittings and tubing. Solutions were introduced into the central channel using model 22 syringe pumps (Harvard Apparatus, Saint Laurent, PQ, Canada). For all experiments shown here, the analyte-to-buffer inlet flow rate ratio was 1:9. The analyte outlet was connected to a fused-silica capillary (length 24 cm, i.d.  $100\ \mu\text{m}$ , Polymicro Technologies, Phoenix, AZ). In optical experiments, the analyte was transferred into a microfuge tube for off-line analysis. In ESI-MS experiments, the sample outlet capillary was connected on-line to the ESI source of the mass spectrometer.

**Optical Experiments.** These were carried out on a Cary 100 Bio spectrophotometer (Mississauga, ON, Canada). In separate trials,  $100\ \mu\text{M}$  cyt *c* or  $80\ \text{mM}$   $\text{KMnO}_4$  in water was injected through the analyte inlet, while water was injected into the buffer inlet. The  $100\text{-}\mu\text{L}$  portions of the analyte outlet stream were collected and diluted 10-fold in distilled water prior to analysis. To determine the extent to which the analyte was retained through the desalting process, the concentration of analyte in the sample outlet stream was compared to the initial concentration. For protein samples, absorbance measurements were taken at  $280\ \text{nm}$  ( $\epsilon_{280} = 10\ 810\ \text{M}^{-1}\ \text{cm}^{-1}$ ) while the  $\text{KMnO}_4$  absorbance was measured at  $525\ \text{nm}$  ( $\epsilon_{525} = 2455\ \text{M}^{-1}\ \text{cm}^{-1}$ ).

**ESI-MS Experiments.** These were carried out on an API 365 triple quadrupole mass spectrometer (MDS-Sciex, Toronto, ON, Canada). The orifice and ring voltages were set to 20 and 200 V, respectively, while the source was held at 5.5 kV relative to ground. All spectra shown were acquired under identical condi-

tions, representing the sum of 10 scans using a dwell time of 2 ms and a step size of  $0.1\ m/z$  units. A custom source assembly was used to accommodate the microchannel chip, and the final sample outlet stream was injected directly into the mass spectrometer.

**Safety Considerations.** Like any experimental technique that is based on ESI-MS, the method described here involves the use of high electric potentials. Precautions should be taken to avoid contact with the ESI source capillary and with the components of the ion sampling interface of the mass spectrometer during operation.

## THEORY AND MODELING

**Laminar Flow Profile.** For a discussion of the microfluidic device used here, it is convenient to introduce a Cartesian coordinate system that has its origin located where the centerlines of the inlet holes intersect with the centerline of the channel (Figure 1). The channel width, depth, and length are denoted as  $2X$ ,  $2Y$ , and  $Z$ , respectively. The flow pattern inside the channel is assumed to be laminar, characterized by a maximum velocity,  $v_{\text{max}}$ , in the centerline of the channel, and a zero flow velocity at the channel walls. The dependence of the flow velocity on the  $x$  and  $y$  coordinates may be expressed as<sup>39</sup>

$$v(x,y) = v_{\text{max}} \left(1 - \left(\frac{|x|}{X}\right)^{n_x}\right) \left(1 - \left(\frac{|y|}{Y}\right)^{n_y}\right) \quad (1)$$

where the relationship between  $v_{\text{max}}$  and the average flow velocity,  $v_{\text{av}}$ , is given by

$$v_{\text{max}} = v_{\text{av}} \left(\frac{n_x + 1}{n_x}\right) \left(\frac{n_y + 1}{n_y}\right) \quad (2)$$

The factors  $n_x$  and  $n_y$  depend on the aspect ratio  $a = 2Y/2X$ , as discussed in ref 39. For the device discussed here,  $2X = 30\ \mu\text{m}$  and  $2Y = 100\ \mu\text{m}$ , such that  $a = 3.33$ . The resulting values are  $n_x = 2.0$  and  $n_y = 4.40$ . The total flow rate inside the channel,  $\dot{V}_{\text{tot}}$ , is given by  $\dot{V}_{\text{tot}} = \dot{V}_{\text{analyte}} + \dot{V}_{\text{buffer}}$ , where  $\dot{V}_{\text{analyte}}$  and  $\dot{V}_{\text{buffer}}$  are the flow rates at which analyte and buffer solution, respectively, are injected. The average flow velocity is defined as

$$v_{\text{av}} = \dot{V}_{\text{tot}}/A \quad (3)$$

where  $A$  is the cross-sectional area of the channel. Equation 1 is valid only for fully developed laminar flow, which is encountered after the liquid has passed a certain entrance length  $Z_{\text{ent}} \approx 2.4A/P$ , where  $P$  is the channel perimeter.<sup>40</sup> The value of  $Z_{\text{ent}}$  predicted by this relationship is in the submillimeter range. Given that the channel has a total length of  $Z = 5\ \text{cm}$ , entrance length effects are considered to be negligible for this study, and the modeling described below is carried out by assuming fully developed laminar flow.

For a 1:9 analyte-to-buffer injection ratio, the analyte solution occupies a relatively narrow layer along the left-hand side of the

(39) Shah, R. K.; London, A. L. In *Advances in Heat Transfer*; Irvine, T. F., Hartnett, J. P., Eds.; Academic Press: New York, 1978; pp 196–222.

(40) Nguyen, N.-T.; Wereley, S. T. In *Fundamentals and Applications of Microfluidics*; Artech House: Boston, 2002; pp 11–62.

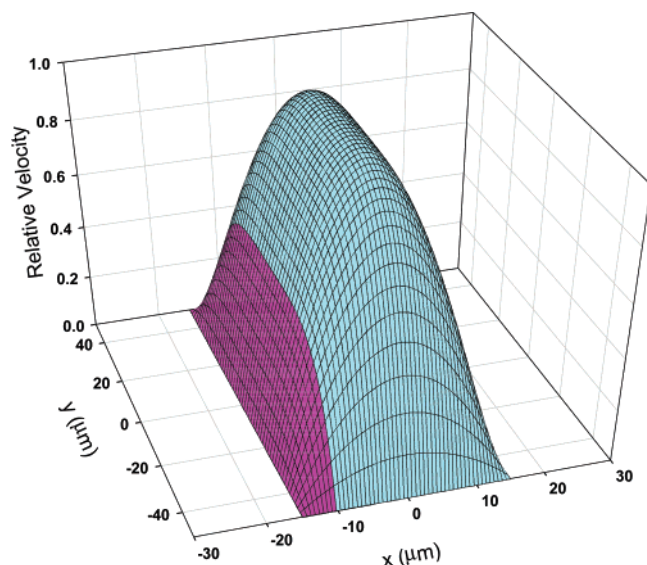


**Figure 2.** Normalized laminar flow velocity profile for the desalter channel used in this work, calculated based on eq 1. The pink region on the left-hand side represents the portion of the profile occupied by the analyte flow layer. The analyte flow layer width was determined based on eq 4.

channel. In a hypothetical plug-flow situation, this layer would encompass 10% of the channel width. The characteristics of the laminar flow profile, however, lead to an analyte layer that is considerably wider, because the proximity to the channel wall implies below-average flow velocities. The location of the boundary separating analyte and buffer,  $X_{\text{boundary}}$ , can be calculated numerically based on

$$\dot{V}_{\text{analyte}} = \int_{-X}^{X_{\text{boundary}}} \int_{-Y}^Y v(x,y) dx dy \quad (4)$$

This relationship predicts that a 1:9 injection ratio will result in an analyte layer occupying ~17% of the total channel width (Figure 2).

**Desalting Simulations.** The convective flow pattern discussed in the preceding section does not take into account diffusion effects, which provide the basis of the desalting method presented here. The combined effects of convection and diffusion can be simulated by an iterative computer modeling approach.<sup>41</sup> The dynamics of the desalting device are described by assuming that during each iteration time interval,  $\Delta t$ , the “particles” (protein and salt) inside the channel are advanced due to laminar flow in the  $z$ -direction by

$$\Delta z_{\text{flow}} = v(x,y)\Delta t \quad (5)$$

In addition, every particle undergoes a diffusive displacement,  $\Delta r$ , that is taken as

$$\Delta r = \sqrt{6D\Delta t} \quad (6)$$

where  $D$  is the diffusion coefficient of the respective molecular

species. Picking two angles,  $\theta$  and  $\phi$ , at random with  $0 \leq \theta < \pi$  and  $0 \leq \phi < 2\pi$ , the diffusive displacement of every particle can be expressed in spherical polar coordinates as

$$\begin{aligned} \Delta x_{\text{diff}} &= \Delta r \sin \theta \cos \phi \\ \Delta y_{\text{diff}} &= \Delta r \sin \theta \sin \phi \\ \Delta z_{\text{diff}} &= \Delta r \cos \phi \end{aligned} \quad (7)$$

such that the iterative increments in the  $x$ ,  $y$ , and  $z$  directions are given by  $\Delta x_{\text{diff}}$ ,  $\Delta y_{\text{diff}}$ , and  $(\Delta z_{\text{diff}} + \Delta z_{\text{flow}})$ , respectively. The iteration time interval was typically chosen as  $\Delta t = 1$  ms, with the number of both protein and salt particles being in the range of  $10^5$ . The contents of the desalter were confined to the channel volume through elastic collisions with the walls. Simulations were performed by using a protein diffusion coefficient of  $1.4 \times 10^{-10} \text{ m}^2 \text{ s}^{-1}$ , corresponding to cyt *c*, a relatively small (12.4 kDa) protein.<sup>42</sup> The salt diffusion coefficient was taken as that of NaCl,  $1.6 \times 10^{-9} \text{ m}^2 \text{ s}^{-1}$ .<sup>43</sup>

Figure 3 illustrates the diffusion behavior of protein and salt for various time points during the simulation. The salt rapidly diffuses across the width of the channel, whereas the protein remains close to its original range of  $x$ -values. These data illustrate the principal feasibility of the proposed desalting process. For example, if the analyte outlet were to sample a layer corresponding to the  $x$ -range of  $-15$  to  $-8 \mu\text{m}$ , it would collect most of the protein but only a fraction of salt that was originally present in the analyte solution.

To quantify the performance of the desalter, we define the efficiency,  $E$ , as the relative concentration of protein divided by the relative concentration of salt in the analyte outlet stream

$$E = \frac{[P_{\text{out}}] [S_{\text{in}}]}{[P_{\text{in}}] [S_{\text{out}}]} \quad (8)$$

where  $[P_{\text{out}}]$  and  $[P_{\text{in}}]$  are the concentrations of protein in the analyte outlet and inlet solutions, respectively. The salt concentrations  $[S_{\text{out}}]$  and  $[S_{\text{in}}]$  are defined analogously.

**Efflux Ratio and Protein Residence Time.** One parameter that affects the desalter performance is the analyte-to-buffer efflux ratio, which can be chosen independently of the 1:9 injection ratio. The efflux ratio determines the width of the layer sampled by the analyte outlet stream. In practice, this ratio can be controlled by the differential back pressure at the two outlet channels. Simulations indicate that the desalting efficiency increases with decreasing analyte-to-buffer efflux ratio. For a total flow rate of  $225 \mu\text{L}/\text{min}$ , an efflux ratio of 1:9 results in  $E = 4.6$ , whereas an  $E$ -value of 5.4 is found for a ratio of 1:44 (Figure 4). However, operating the device at very small analyte-to-buffer efflux ratios is impractical for several reasons. Both the absolute volume of the analyte solution and the total amount of protein recovered under these conditions are very low. Another point to consider is the average residence time,  $\langle a \rangle$ , of the proteins inside the channel, which also

(42) Clark, S. M.; Leait, D. G.; Konermann, L. *Rapid. Commun. Mass Spectrom.* **2002**, *16*, 1454–1462.

(43) Lide, D. R. *CRC Handbook of Chemistry and Physics*, 82nd ed.; CRC Press: Boca Raton, FL, 2001.

(41) Konermann, L. *J. Phys. Chem. A* **1999**, *103*, 7210–7216.

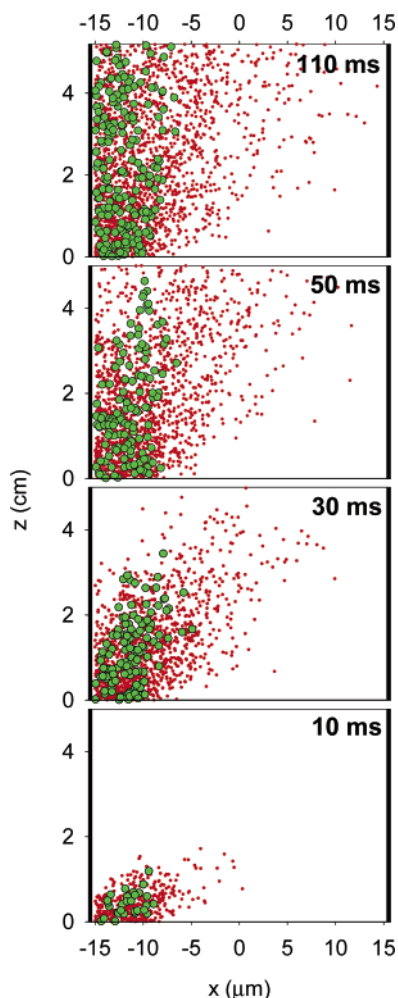


**Figure 3.** Simulation of the convection and diffusion processes inside the desalter channel for a total flow rate of  $225 \mu\text{L}/\text{min}$  and an analyte-to-buffer injection ratio of 1:9. The panels represent top views of the desalter (looking down the  $y$ -axis), for different time points, as indicated. Red dots stand for salt (diffusion coefficient  $D = 1.6 \times 10^{-9} \text{ m}^2 \text{ s}^{-1}$ ), and green circles represent protein ( $D = 1.4 \times 10^{-10} \text{ m}^2 \text{ s}^{-1}$ ).

increases with decreasing analyte-to-buffer efflux ratio (Figure 4). A small efflux ratio, therefore, is detrimental to rapid desalting. For the following simulations, as well as for the experimental data discussed later, a compromise was made in choosing an analyte-to-buffer efflux ratio of 1:12.2, corresponding to analyte and waste outlet flow rates of 17 and  $208 \mu\text{L}/\text{min}$ , respectively. Under these conditions, the simulations predict a desalting efficiency  $E = 4.8$ , and an average protein residence time  $\langle a \rangle = 63 \text{ ms}$ .

Calculation of  $\langle a \rangle$  was performed by following an approach developed previously.<sup>41</sup> If  $P(a) da$  is the probability that a protein at the distal end of the channel has a residence time (“age”) in the range  $a$  to  $a + da$ , then the average protein residence time is given by

$$\langle a \rangle = \int_0^{\infty} aP(a) da \quad (9)$$

$P(a)$  can be calculated by tracking the residence time of every protein particle exiting via the analyte outlet (Figure 5).

**Total Flow Rate.** The desalting efficiency depends critically on the total flow rate  $\dot{V}_{\text{tot}}$  within the channel. It is instructive to

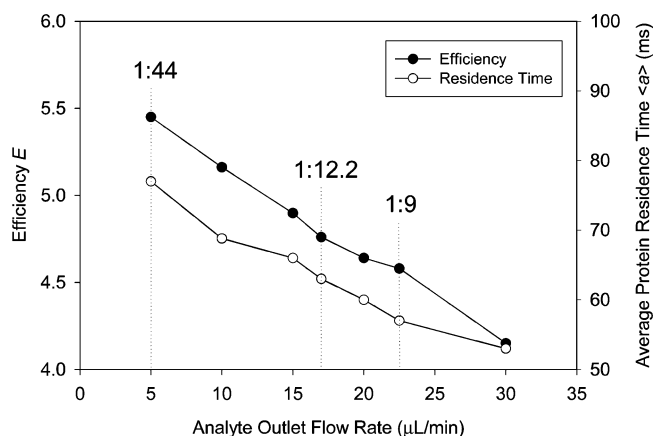


**Figure 4.** Simulated effects of analyte outlet flow rate on the desalting efficiency  $E$  (filled circles) and the average protein residence time inside the channel  $\langle a \rangle$  (open circles), based on the simulation depicted in the preceding figure. Analyte-to-buffer efflux ratios are indicated for some of the data points (dotted lines).

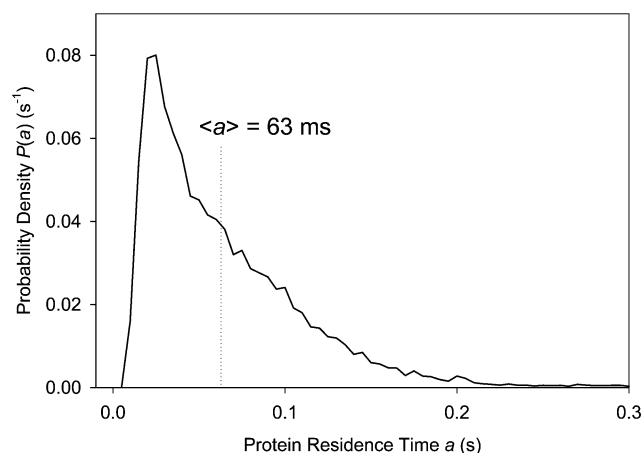


**Figure 5.** Age distribution function  $P(a)$  of proteins exiting the desalter via the analyte outlet for an analyte-to-buffer efflux ratio of 1:12.2 and an inlet ratio of 1:9. The dotted line indicates the average value of this distribution, calculated from eq 9.

discuss three limiting scenarios: (i) Diffusion of the protein is negligible, but diffusion of the salt leads to complete randomization of its  $x$ -positions by the time the solution has traveled through the channel. This scenario represents maximum efficiency conditions, with  $[P_{\text{out}}] = [P_{\text{in}}]$  and  $[S_{\text{out}}] = 0.1[S_{\text{in}}]$ , such that  $E = 10$ . (ii) The flow velocity inside the channel is extremely high, such that diffusion is negligible for both protein and salt due to the short residence time inside the channel. In this case,  $[P_{\text{out}}] = [P_{\text{in}}]$  and  $[S_{\text{out}}] = [S_{\text{in}}]$ , such that  $E = 1$ . (iii) The flow velocity is extremely low, such that the  $x$ -positions of both protein and salt are completely randomized between  $-X$  and  $X$  by the time the solution reaches the distal end of the channel. This scenario implies that  $[P_{\text{out}}] = 0.1[P_{\text{in}}]$  and  $[S_{\text{out}}] = 0.1[S_{\text{in}}]$ , again resulting in  $E = 1$ . An  $E$ -value of unity, therefore, represents a worst-case scenario, i.e., a total lack of desalting performance. This behavior is encountered for both very high and very low flow rates, implying that the efficiency can be maximized by choosing a suitable  $\dot{V}_{\text{tot}}$  value between these two limiting cases. Modeling the desalting process confirms this expectation. According to the data depicted in Figure 6, the device operates at a maximum efficiency of  $\sim 5.0$  in the range around  $120\text{--}250 \mu\text{L}/\text{min}$ . Lower flow rates lead to a

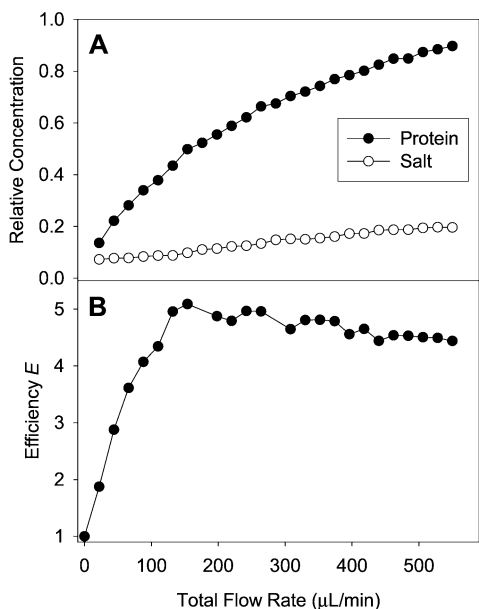


**Figure 6.** Simulated data, describing the effects of the total flow rate on the desalting efficiency. (A) Relative protein concentration,  $[P_{out}]/[P_{in}]$ , and relative salt concentration,  $[S_{out}]/[S_{in}]$ . (B) Desalting efficiency, calculated as  $E = (\text{relative protein concentration})/(\text{relative salt concentration})$ , according to eq 8.

very rapid drop in efficiency, whereas the performance declines more gradually at high flow rates. It is noted that the slightly noisy appearance of the simulated data in Figures 4–6 can be traced back to the random number generator used to model the diffusion processes.

The simulations used do not incorporate the possible onset of turbulence. Although the flow rates and channel dimensions used in our experiments result in Reynolds numbers below 150 for all flow rates used, transitional behavior or even turbulence can occur under these conditions, particularly in the vicinity of the intersection between the circular access holes and the rectangular desalting channel.<sup>40</sup> Also, roughness of the channel walls can decrease the threshold Reynolds number.<sup>44</sup> Consequently, experimental tests are required to validate the model used and to ensure that there is minimal turbulent mixing of the input streams prior to the development of a stable, layered laminar flow.

## RESULTS AND DISCUSSION

**Optical Experiments.** To characterize the performance of the desalting device experimentally, optical studies were carried out using  $\text{KMnO}_4$  and *cyt c* as test compounds.  $\text{KMnO}_4$  has a diffusion coefficient of  $1.8 \times 10^{-9} \text{ m}^2 \text{ s}^{-1}$ , which is close to that of  $\text{NaCl}$  (see theory section, above).<sup>43</sup> For flow rates up to  $225 \mu\text{L}/\text{min}$ , the relative concentrations of both protein and salt exhibit a behavior consistent with that seen in the simulations (Figure 7). The salt, being essentially fully diffused across the channel shows relative concentrations close to the theoretical minimum of 0.1 in this flow rate range. The relative protein concentration shows a pronounced increase up to almost 0.7, reflecting the different diffusion behavior of the two compounds (Figure 7A). At flow rates of  $300 \mu\text{L}/\text{min}$  and above, the protein concentration declines rapidly. This effect is attributed to the onset of turbulent flow,

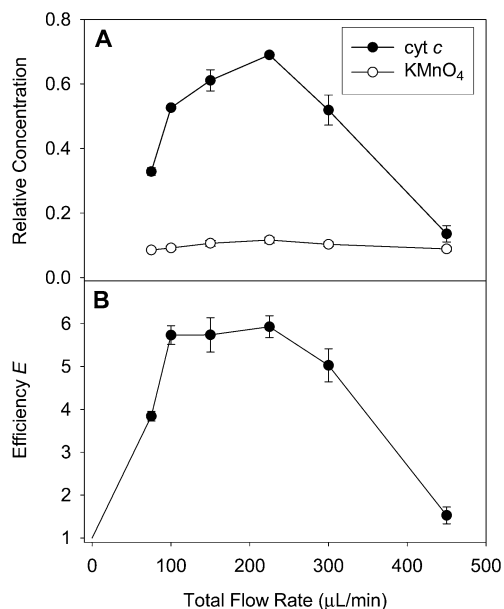


**Figure 7.** Experimentally measured data, describing the effects of the total flow rate on the desalting efficiency. (A) Relative concentrations of *cyt c* and  $\text{KMnO}_4$  at the analyte outlet, determined by UV–vis spectrophotometry. (B) Desalting efficiency  $E$ . Error bars reflect the standard deviations of three independent measurements taken for each data point.

likely in the inlet region of the desalter. The accompanying mixing of analyte and buffer solutions leads to a deterioration of the desalter performance. The data indicate a peak desalting efficiency of  $5.9 \pm 0.3$  at  $225 \mu\text{L}/\text{min}$  (Figure 7B). This slightly exceeds the maximum  $E$ -value around 5, which is expected from the simulations (Figure 6B).

**ESI-MS Desalting Experiments. (1) Cytochrome *c*.** The utility of the device for improving protein mass spectra from high-salt solutions was demonstrated in on-line ESI-MS experiments. All the experiments shown in the remainder of this work were carried out at a total flow rate of  $225 \mu\text{L}/\text{min}$ , using an analyte-to-buffer injection ratio of 1:9 and an analyte-to-buffer efflux ratio of 1:12.2. Aqueous solutions of  $20 \mu\text{M}$  *cyt c* were prepared in 1 mM ammonium acetate containing  $\text{NaCl}$ . It was found that the protein signals were almost completely abrogated at a sodium chloride concentration of 25 mM (Figure 8A). After passing the protein solution through the desalting device, using 1 mM ammonium acetate in water as desalting buffer, a dramatic improvement was observed, and *cyt c* ions in charge states 7+ to 9+ were clearly observable (Figure 8B). Chemical noise in the form of sodium chloride clusters, which were the dominant ionic signals in the spectrum of Figure 8A, are no longer present after the desalting step. However, peak tailing due to  $\text{Na}^+$  and  $\text{NaCl}$  adduction persists.

It is possible to operate two desalting channels in series; i.e., the analyte efflux of the first device can be connected to the analyte injection channel of a second device. This should result in a squared efficiency (more generally,  $E^n$  for  $n$ -stage desalting). As expected, double-stage desalting of the original  $\text{NaCl}$ -contaminated protein solution results in an even more dramatic improvement in signal intensity and signal-to-noise ratio (Figure 8C). These data indicate that each of the two desalting steps increases the spectral quality by roughly 1 order of magnitude.

(44) Morini, G. L. *Microscale Therm. Eng.* **2004**, *8*, 15–30.

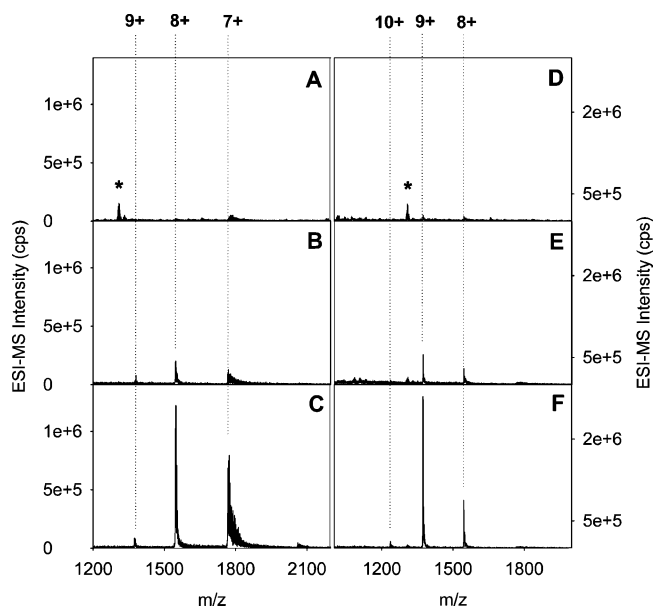


**Figure 8.** ESI mass spectra of solutions initially containing 20  $\mu\text{M}$  cyt *c* and 25 mM NaCl without desalting (A), after single-stage desalting (B), and after double-stage desalting (C). The conditions for panels D–F were analogous to (A–C), except that the initial NaCl concentration was 50 mM, and all solutions contained 0.5% acetic acid. The dominant signal marked with an asterisk in panels A and D can be tentatively assigned to incompletely desolvated clusters  $[\text{NaCl}_{22} + \text{Na}]^+$  and  $[\text{NaCl}_{44} + 2\text{Na}]^{2+}$ .<sup>8</sup> Also shown are the charge states of the observed protein ions.

The experiment was repeated for solutions initially containing 20  $\mu\text{M}$  protein and 0.5% acetic acid. An increased NaCl concentration of 50 mM was necessary to virtually eliminate the protein signals under these slightly acidic conditions (Figure 8D). The desalting buffer used contained the same acetic acid concentration as the protein solution. The intensity and signal-to-noise improvements caused by the desalting device under these conditions are even more notable than in the first example (Figure 8E,F). A high-quality spectrum with very little adduction was observed after double-stage desalting (Figure 8F). In comparison, only very minor signal improvements could be achieved upon simply mixing the salt-contaminated protein solutions with desalting buffer for all cases studied here (data not shown).

**(2) Bradykinin.** The desalting process used here requires the diffusion coefficients of analyte and salt to be significantly different. Consequently, this approach is expected not to be as effective for the desalting of lower molecular weight analytes, such as peptides. To explore this limitation, desalting experiments were conducted on bradykinin, a short peptide consisting of nine amino acid residues (Arg-Pro-Pro-Gly-Phe-Ser-Pro-Phe-Arg, MW 1060), which has a diffusion coefficient of  $\sim 4 \times 10^{-9} \text{ m}^2 \text{ s}^{-1}$ .<sup>29</sup> ESI-MS analysis of a 5  $\mu\text{M}$  bradykinin solution containing 1 mM ammonium acetate and 25 mM NaCl results in a poor mass spectrum that shows an elevated baseline and extensive chemical noise (Figure 9A). Single-stage desalting results in a moderate improvement of the spectral quality, by reducing the chemical noise and by suppressing sodium adduction to the analyte. However, the absolute bradykinin signal intensity does not increase under these conditions (Figure 9B). These observations are in line with the expectation that the relatively high diffusion coefficient of bradykinin does not allow this compound to be sufficiently retained in

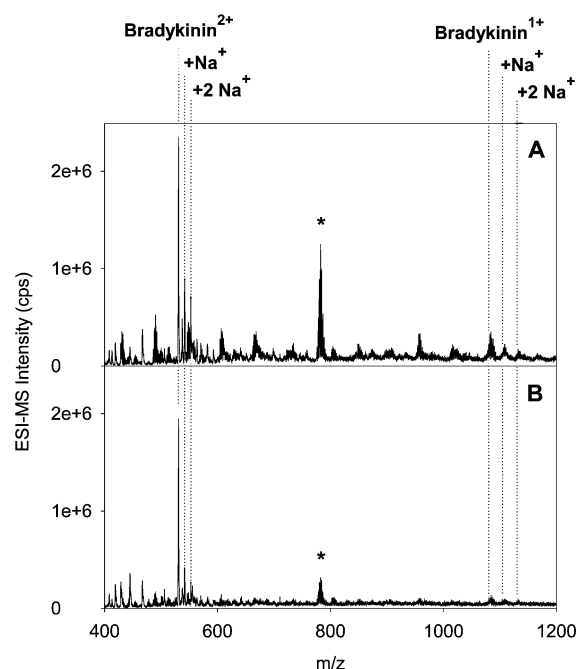


**Figure 9.** ESI mass spectra of 5  $\mu\text{M}$  bradykinin in 25 mM NaCl before (A) and after (B) single-stage desalting. Dotted lines indicate the expected positions of bradykinin  $1^+$  and bradykinin  $2^+$  ions, with one or two  $\text{Na}^+$  bound. The dominant chemical noise signal, marked with an asterisk is likely due to incompletely desolvated salt clusters  $[\text{NaCl}_{13} + \text{Na}]^+$  and  $[\text{NaCl}_{26} + 2\text{Na}]^{2+}$ .<sup>8</sup>

the analyte flow layer. It appears that efficient desalting by the technique presented here requires the diffusion coefficients of salt and analyte to differ by 1 order of magnitude or more.

## CONCLUSIONS

We have demonstrated a method for the ultrarapid on-line purification of macromolecule solutions. The technique relies on the differential exchange of analyte and low molecular weight contaminants, such as salts, between two laminar flow layers. For the cyt *c*/NaCl example studied here, roughly 70% of the protein is retained during single-stage desalting, while 90% of the salt is removed. The loss of 30% of protein may appear to be a potential limitation of this technique. However, some loss is also expected to occur for other purification methods. In addition, the approach used here eliminates the problem of protein adsorption to dialysis membranes. Since no membrane is used, the technique takes full advantage of rapid diffusion on the microscale. Consequently, desalting occurs over a period of only  $\sim 60$  ms, which is more than 2 orders of magnitude faster than other rapid desalting methods.<sup>24–27,45</sup> This greatly enhanced speed could drastically reduce per-sample analysis time in high-throughput studies. It also raises the possibility of maintaining natively like salt conditions for studies on intricate biological systems until immediately prior to ESI-MS analysis, which is desirable for protein structure/function studies and for on-line time-resolved experiments. Additionally, the device may facilitate the rapid analysis of proteins and other macromolecules in biological matrixes, such as urine or blood, or in complex mixtures. It may also be useful for applications

(45) Xiang, F.; Lin, Y.; Wen, J.; Matson, D. W.; Smith, R. D. *Anal. Chem.* **1999**, *71*, 1485–1490.

related to on-line process monitoring. Other areas of interest that are not directly related to ESI-MS include rapid buffer exchange steps, e.g., during protein purification.

Reduction of the time required for a certain step during an analytical procedure often shifts the bottleneck to other aspects of the technique, such as the delivery of sample or transfer to the detector.<sup>46,47</sup> The present work focuses on the characterization of the desalting mechanism; no particular efforts were made to ensure rapid transfer from the desalter to the ESI source. Consequently, desalting and ionization of the analyte were separated by several seconds. This gap could be virtually eliminated by employing micronozzles<sup>48</sup> or porous polymer monoliths<sup>49</sup> for on-chip ESI. Similarly, the serial coupling of two desalting stages was performed here by using a standard PEEK transfer line. To minimize the overall sample processing time, multiple desalting stages could be coupled in serial mode on a single chip. Another interesting possibility is the usage of a

geometry that has the analyte stream sandwiched between two layers of desalting buffer, analogous to hydrodynamic focusing devices for kinetic measurements.<sup>22,23</sup> Such an arrangement could potentially result in even shorter desalting times, since the analyte solution would travel as an extremely narrow layer with the maximum velocity along the centerline of the laminar flow channel, instead of being confined to a slow region adjacent to a wall. These developments are currently being pursued in our laboratory, with the goal of using these devices for time-resolved ESI-MS studies on the kinetics and dynamics of biological systems.<sup>30,50</sup>

#### ACKNOWLEDGMENT

We thank Derek G. Leist and Suya Liu for helpful discussions, and Paul Kebarle for sending us a preprint of ref 11 ahead of publication. This work was financially supported by the Natural Sciences and Engineering Research Council of Canada (NSERC), the Canada Foundation for Innovation (CFI), the Provincial Government of Ontario, The University of Western Ontario, and the Canada Research Chairs Program.

Received for review May 23, 2005. Accepted August 26, 2005.

AC050902O

(46) Stuart, J. N.; Sweedler, J. V. *Proc. Natl. Acad. Sci. U.S.A.* **2003**, *100*, 3545–3546.

(47) Plenert, M. L.; Shear, J. B. *Proc. Natl. Acad. Sci. U.S.A.* **2003**, *100*, 3853–3857.

(48) Bings, N. H.; Wang, C.; Skinner, C. D.; Colyer, C. L.; Thibault, P.; Harrison, D. J. *Anal. Chem.* **1999**, *71*, 3292–3296.

(49) Koerner, T.; Turck, K.; Brown, L.; Oleschuk, R. D. *Anal. Chem.* **2004**, *76*, 6456–6460.

(50) Wilson, D. J.; Konermann, L. *Anal. Chem.* **2003**, *75*, 6408–6414.